

# High-Temperature Creep Behavior of SiOC Glass-Ceramics: Influence of Network Carbon Versus Segregated Carbon

Emanuel Ionescu,<sup>‡,†</sup> Corneliu Balan,<sup>§,†</sup> Hans-Joachim Kleebe,<sup>‡</sup> Mathis M. Müller,<sup>‡</sup> Olivier Guillon,<sup>¶</sup> Daniel Schliephake,<sup>||</sup> Martin Heilmaier,<sup>||</sup> and Ralf Riedel<sup>‡</sup>

<sup>‡</sup>Fachbereich Material- und Geowissenschaften, Technische Universität Darmstadt, Jovanka-Bontschits-Strasse 2, Darmstadt D-64287, Germany

<sup>§</sup>Hydraulics Department, Politehnica University Bucharest, Splaiul Independentei nr. 313, Bucharest 060042, Romania

<sup>¶</sup>Otto Schott Institute of Materials Research, Friedrich Schiller University Jena, Löbdergraben 32, Jena D-07743, Germany

<sup>||</sup>Institut für Applied Materials, Karlsruher Institut für Technologie, Engelbert-Arnold-Strasse 4, Karlsruhe D-76131, Germany

Three silicon oxycarbide samples with different carbon contents are analyzed in the present study with respect to their high-temperature creep behavior. The tests were performed in compression at 1100°C, 1200°C, and 1300°C; in this temperature range the mechanism of creep relies on viscoelastic flow within the samples and has been modeled with the Jeffreys viscoelastic model. After the release of the applied mechanical stress, a viscoelastic recovery behavior was observed in all samples. The creep behavior of the investigated samples indicates two rheological contributions in SiOC: (i) a high viscous answer, coming from the silica-rich network, and (ii) an elastic response from the segregated carbon phase within the samples. Furthermore, two distinct effects of the carbon phase on the HT creep behavior of SiOC were identified and are discussed in the present paper: the effect of the carbon presence within the SiOC network (the “carbide” carbon), which induces a significant increase in the viscosity and a strong decrease in the activation energy for creep, as compared to vitreous silica; and the influence of the segregated carbon phase (the “free” carbon), which has been shown to affect the viscosity and the activation energy of creep and dominates the creep behavior in phase-separated silicon oxycarbides.

## I. Introduction

SILICON oxycarbide-based ceramics (also referred as to black glasses) are materials which can be described as consisting of an amorphous network of  $\text{SiO}_x\text{C}_{4-x}$  ( $x = 0-4$ ) tetrahedra which formally might be the result of the incorporation of carbon into silica glass. Although the first attempts to incorporate carbon into silica date back to the early 50s,<sup>1</sup> silicon oxycarbide glasses have been synthesized only since less than three decades, since no suitable preparative access to the Si–O–C ternary system could be realized either by reacting carbon with silica or by oxidizing silicon carbide. Thus, the only appropriate synthetic approach for SiOC ceramic relies on the use of sol–gel precursors based on the organically modified alkoxy silanes [e.g.,  $\text{R}_x\text{Si}(\text{OR}')_4$  with R and R' being alkyl or aryl groups] as well as of polyorganosiloxanes.<sup>2</sup> Both types of preceramic precursors exhibit Si–C and Si–O bonds within their backbone, which are

preserved upon polymer-to-ceramic transformation. By varying the nature and the amount of the organic substituents within the structure of the preceramic precursors, the composition of SiOC-based materials (i.e., the amount of carbon present within the ceramic network) can be controlled and has been shown to have a strong influence on their properties.<sup>2-4</sup> Thus, silicon oxycarbides remain amorphous up to  $T = 1200^\circ\text{C}$ ,<sup>5</sup> present unique creep resistance up to high temperatures<sup>6-9</sup> and excellent behavior in oxidative and corrosive environments.<sup>2</sup> The incorporation of additional elements into the Si–O–C systems can lead to a further improvement of those properties.<sup>10</sup>

Especially the excellent creep behavior of SiOC glasses at temperatures beyond 1000°C is rather unique and makes this class of materials highly interesting for high and ultrahigh temperature applications. It is known that glasses exhibit thermo-mechanical properties which strongly correlate to the strength of their bonds as well as to the topology (or “cross-linking”) of their atomic network.<sup>7</sup> This has been shown for silicate glasses in which oxygen was partially substituted by nitrogen<sup>11</sup>: upon substituting 20 at% of  $\text{O}^{2-}$  with  $\text{N}^{3-}$ , an increase of 30% in Young’s modulus was reported, whereas the viscosity increases significantly (two orders of magnitude)<sup>12</sup>; this remarkable effect of the nitrogen substitution has been related to the increase in the average coordination number in the glass network.<sup>13</sup>

Similarly, in silicon oxycarbide glasses divalent oxygen is replaced by tetravalent carbon, which was shown to strongly increase the glass transition temperature from 1170°C (as for vitreous silica)<sup>14</sup> to temperatures beyond 1350°C–1400°C for SiOC glass.<sup>7,9</sup>

Several studies dealing with the role of carbon in SiOC glasses on their HT creep behavior were published within the last 15 yr.<sup>6-9</sup> It was observed that the incorporation of carbon within silica glass not only affects its viscosity/glass transition range but also induces an (an)elastic component into the response of the material upon mechanical loading at high temperatures.<sup>8,15</sup> Thus, a visco(an)elastic behavior of SiOC materials was reported at temperatures beyond 1000°C and was related to a unique nano-heterogeneous network topology of SiOC, which consists of silica-containing nanodomains (which would respond mainly in a viscous manner upon HT mechanical load) embedded within a graphene-like carbon network acting elastically under load at high temperature.<sup>8,16</sup> More recent studies (based on solid-state nuclear magnetic resonance, MAS NMR, and HT creep data) indicate that the microstructure of SiOC glasses may be described as consisting of two interpenetrating continuous networks, one viscous silica continuous phase and an elastic

V. Sglavo—contributing editor

Manuscript No. 34559. Received February 18, 2014; approved July 28, 2014.

<sup>†</sup>Authors to whom correspondence should be addressed.  
e-mails: ionescu@materials.tu-darmstadt.de and corneliu.balan@upb.ro

carbon network.<sup>9,17</sup> This microstructural model was used to explain for instance the HT creep behavior of hot-pressed SiOC, SiZrOC, and SiHfOC materials.<sup>9</sup>

To support the proposed microstructural model, high temperature creep data of SiOC materials with three different carbon contents were numerically modeled using the Jeffreys viscoelastic model. The HT creep behavior can be explained by the proposed structure of two interpenetrating networks (one viscous and one elastic). Furthermore, the effect of the “carbide” carbon and of the segregated carbon phase on the HT creep behavior of SiOC glasses can clearly be distinguished.

## II. Experimental Procedure

### (1) Materials Synthesis and Processing

The preparation of the monolithic ceramic samples was performed by hot-pressing the corresponding ceramic powders at 1600°C in argon atmosphere. The sample MK was prepared starting from a commercially available polysilsesquioxane (Belsil PMS MK, Wacker, Burghausen, Germany) which was pyrolyzed at 900°C in argon.<sup>9,18</sup> The precursors for the samples SG1 and SG2 were prepared by sol-gel processing starting from two different ratios of methyl-diethoxysilane and triethoxysilane, as described by Rouxel *et al.*<sup>7</sup> Subsequently, the precursors were pyrolyzed at 900°C in argon. The obtained ceramic powders were ground in a planetary ball mill, sieved (mesh size 32  $\mu\text{m}$ ) and subsequently hot-pressed (Pressvac; Elatec Inc, Wilmington, DE) at 1600°C in a graphite die (20 mm diameter) to dense monoliths (30 MPa, Ar atmosphere, dwell 30 min).

### (2) Materials Characterization

Elemental analyses of the samples were performed by hot gas extraction (Mikrolabor Pascher, Remagen, Germany). Powder X-ray diffraction ( $\text{CuK}\alpha$ ) was performed in transmission mode on a Stadi P diffractometer from STOE (Darmstadt, Germany) equipped with a (111) germanium single-crystal monochromator and a linear PSD-detector. Transmission electron microscopy (TEM) imaging was performed using a CM20STEM instrument (FEI, Eindhoven, the Netherlands) operating at 200 kV on TEM-foils obtained from the bulk samples. Sample preparation followed standard ceramographic techniques involving cutting, ultrasonic drilling, dimpling, and Ar-ion thinning to perforation followed by light carbon coating to minimize charging under the incident electron beam. A laser-assisted high-resolution loading dilatometer (with a resolution of 50 nm and an accuracy of 0.5  $\mu\text{m}$ ) was used for the compressive creep experiments, which were performed in air atmosphere.<sup>19</sup> A programmable heating controller and high-temperature cylindrical split furnace (max. operation temperature 1500°C) equipped with four MoSi<sub>2</sub> heating elements was used. The temperature was controlled by a programmable heating system and a Type R thermocouple in contact with the sample. The samples were placed between two plane parallel sapphire plates. The furnace was heated up to different temperatures and the force was varied during the dwell time to apply 10, 25, and 50 MPa (see in Table I the sample dimensions and the applied forces during the creep experiment).

### (3) The Viscoelastic Jeffreys Model

At temperatures below 1000°C, the monolithic SiOC ceramics behave like viscoelastic solids; whereas above that temperature and under high compression stresses, the samples disclose well-defined secondary creep behavior, which is usually associated to the flow at very low strain rates. In our tests, it is assumed that beyond the experimental time  $t_e^{(1)}$ , (i.e.,  $t > t_e$ ) the strain rate  $\dot{\epsilon}$  is maintained constant under the

**Table I. Sample Dimensions and Forces Used for Mechanical Loading During the HT Creep Experiments. Due to Different Dimensions of SG1, the Applied Force was Adjusted to Provide the Same Pressure on Sample During the Creep Experiments**

Sample	Sample dimensions (mm × mm × mm)	Applied force (N)		
		For 10 MPa pressure	For 25 MPa pressure	For 50 MPa pressure
SG1	2 × 2.1 × 4	41	102.5	205
SG2	3 × 3 × 5	90	225	450
MK	3 × 3 × 5	90	225	450

applied constant stress  $\sigma = \sigma_0$ , thus the samples exhibit secondary creep (at  $0 < t < t_e^{(1)}$  the samples show primary creep, that is, the strain rate is steadily decreasing with time). However, after a long period of loading, the samples might disclose again primary creep behavior (e.g., at  $t > t_e^{(2)} > t_e^{(1)}$   $\dot{\epsilon} \rightarrow 0$  and the deformation eventually achieves the steady state (i.e.,  $\epsilon \rightarrow \epsilon_{st}$ ).

A complete description of the rheology of multicomponent viscoelastic materials with one single 3D constitutive relation is very difficult, since nonlinear terms have to be considered in the model; however, this is not the goal of the present work. In the case of dynamic processes with simple kinematics (as pure shear or compression), a more convenient approach is to use for each region different linear models, which at some critical states of stress or strains can be coupled with each other by a Saint Venant element. A corresponding analogical model is shown in Fig. 1. The linear behavior of a viscoelastic fluid (which discloses primary and secondary creep as well as strain recovery at  $\sigma = 0$ ) is represented by the Jeffreys-1 model (a viscous Newtonian element connected in parallel with a Maxwell fluid), whereas a Jeffreys-2 model results from connecting in parallel a Maxwell fluid with an elastic (Hooke) element (proper to describe the viscoelastic solid behavior). Additionally, viscoelastic solids can be described with the Burgers 4-constants model, which consists of a Maxwell element connected in parallel with a Kelvin-Voigt element (see Fig. 1 as for the Saint Venant element being switched on).<sup>20</sup>

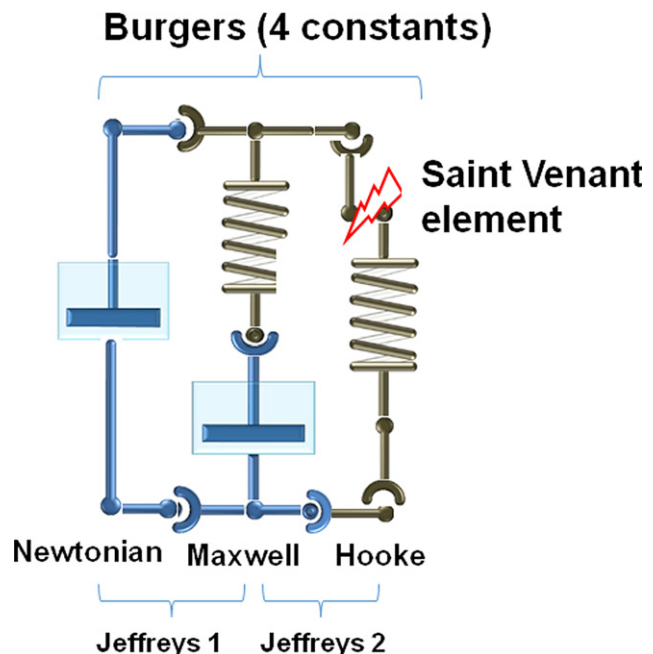


**Fig. 1.** Representation of different linear viscoelastic models.

The graphical representations of the creep behavior of Jeffreys-1 and Jeffreys-2 linear viscoelastic models are given in Fig. 2,<sup>20</sup> see also Ref. [8]. Secondary creep is disclosed only for the Jeffreys-1 model; whereas the Jeffreys-2 model exhibits only primary creep. However, the two models might look similar for some regions with very low shear rates where experimental data corresponding to secondary creep for the Jeffreys-1 model and to primary creep of the Jeffreys-2 model can have similar numerical values.

In our work, the region where the samples under investigations typically disclose primary creep followed by secondary creep has been modeled with the Jeffreys-1 relation,<sup>20</sup>

$$\frac{\eta_m}{E} \dot{\sigma} + \sigma = \frac{\eta_m \eta_v}{E} \ddot{\varepsilon} + (\eta_m + \eta_v) \dot{\varepsilon} \quad (1)$$

where a pure Newtonian fluid with viscosity  $\eta_v$  is connected in parallel with a Maxwell element described by a viscosity  $\eta_m$  and an elastic modulus  $E$ . In Eq. (1)  $\sigma$  represents the stress and  $\varepsilon$  is the corresponding strain ( $\dot{\varepsilon}$  and  $\ddot{\varepsilon}$  being its first and second time derivatives, respectively). The complete 3D formulation of the Jeffreys model was reported by Balan and Tsakmakis in Ref. [20], but its solution in our case involves a numerical procedure which needs supplementary data to the present experiments (e.g., tests under controlled strain or strain rate).

As the stress is maintained constant during the creep test duration, the exact nondimensional solution of Eq. (1) is given by Eq. (2):

$$\varepsilon = (\dot{\varepsilon}_0 - \dot{\varepsilon}_{st})(1 - e^{-t/a}) + \dot{\varepsilon}_{st} t/a \quad (2)$$

where  $a$  is the time scale (i.e.,  $a = \frac{\eta_m \eta_v}{(\eta_m + \eta_v) E}$ ),  $\dot{\varepsilon}_{st}$  is the steady strain rate corresponding to the applied stress  $\sigma_0$  ( $\dot{\varepsilon}_{st} = \frac{\sigma_0}{\eta_m + \eta_v} \cdot a$ ) and  $\varepsilon_0$  is the nondimensional initial strain rate.

The Jeffreys-1 viscoelastic model was used to fit the high-temperature creep data of the three SiOC-based samples within the present study, to further substantiate their microstructural description which involves the presence of two interpenetrating networks, a viscous silica network and an elastic carbon network.<sup>8,9,16,17</sup>

Since the tested samples are complex multicomponent materials, it is not expected to rationalize their complete rhe-

ological behavior with simple linear constitutive relations, such as the Jeffreys or Burgers models. However, we consider that Eq. (1) and its solution (i.e., Eq. (2)) have the capability to provide a fair representation of the high-temperature evolution of the samples under compression creep conditions.

### III. Results and Discussion

The prepared samples MK, SG1, and SG2 were investigated with respect to their chemical and phase composition as well as their microstructure by using elemental analysis, spectroscopic methods (Raman, NMR), and electron microscopy techniques.

The X-ray diffraction patterns of the prepared samples are shown in Fig. 3. All three samples are considered to be mainly X-ray amorphous; however, broad peaks corresponding to  $\beta$ -SiC were observed in all XRD patterns.

The samples were also investigated by <sup>29</sup>Si MAS NMR spectroscopy. The spectra of MK, SG1 as well as of SG2 are very similar (Fig. 4) and exhibit two signals at approximately -18 and -110 ppm, which were assigned to SiC<sub>4</sub> and SiO<sub>4</sub> sites, respectively.<sup>21</sup> Usually, SiOC materials exhibit a short-range structure consisting of Si atoms forming SiO<sub>x</sub>C<sub>4-x</sub> tetrahedra. Consequently, the <sup>29</sup>Si NMR spectrum of a SiOC glasses exhibit beside the two resonance of SiO<sub>4</sub> and SiC<sub>4</sub> sites additional resonances corresponding to "mixed bonds" tetrahedra, that is, SiOC<sub>3</sub> (+6 ppm), SiO<sub>2</sub>C<sub>2</sub> (-35 ppm), and SiO<sub>3</sub>C (-70 ppm).<sup>22</sup> The absence of the signals related to SiO<sub>x</sub>C<sub>4-x</sub> mixed bonds indicates that the prepared samples are phase-separated, multiphase systems containing amorphous silica, silicon carbide, and excess carbon.<sup>9</sup>

TEM investigation on the prepared samples supported the XRD and NMR findings, indicating the presence of turbostratic carbon and SiC nano-precipitations within an amorphous silica-rich matrix (Fig. 5). The segregated turbostratic carbon showed a high aspect ratio (10–20) and the SiC nano-particles exhibited sizes of only a few nanometers.

Based on the elemental analysis data of the three investigated SiOC samples (Table II) and considering them being phase-separated as revealed by the <sup>29</sup>Si MAS NMR and TEM results (i.e., consisting of amorphous silica, SiC and excess carbon), a formal phase composition was estimated. Thus, for an empirical formula Si<sub>x</sub>O<sub>y</sub>C<sub>z</sub>, the oxygen is bonded only to silicon to form the silica phase (i.e.,  $\frac{y}{2}$  mol silica), the remaining silicon is bonded to carbon to yield silicon carbide ( $x - \frac{y}{2}$  mol) and the remaining carbon (i.e.,  $z - (x - \frac{y}{2})$  mol) represents the segregated carbon

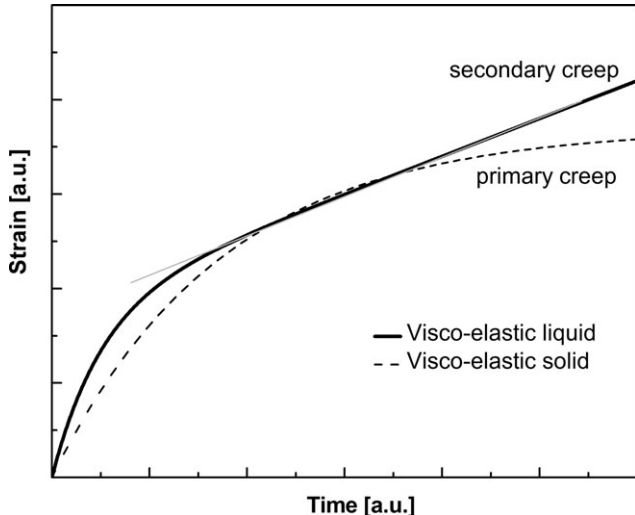


Fig. 2. Strain as function of time under a constant stress for a Jeffreys-1 fluid model (continuous line) and its viscoelastic solid analogue Jeffreys-2 model (dashed line).

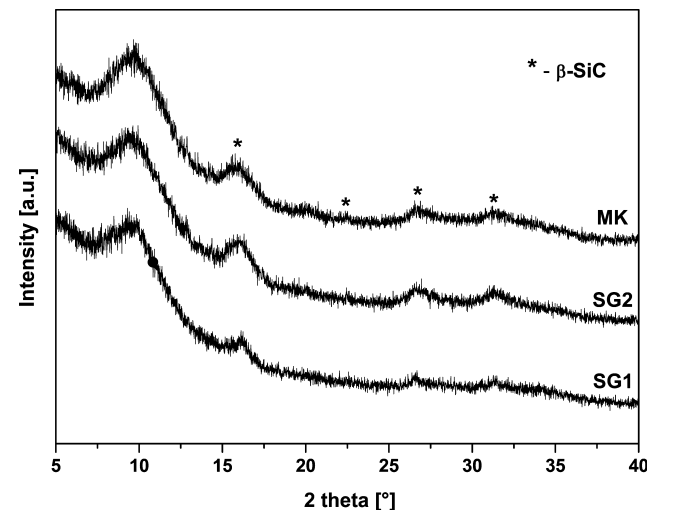
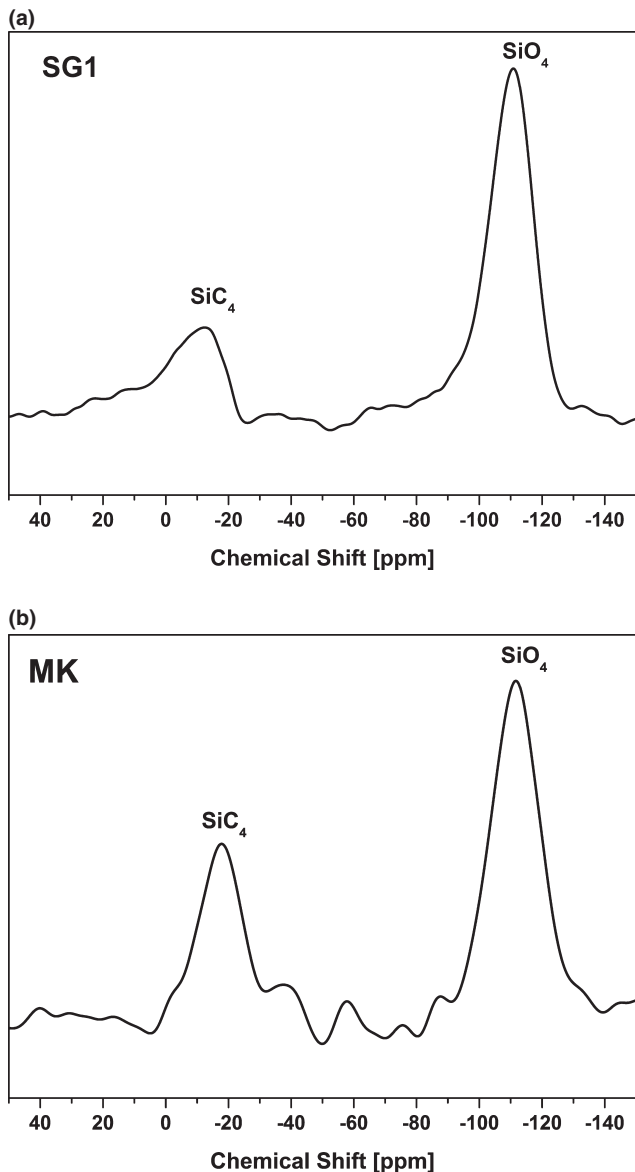


Fig. 3. XRD patterns of SG1, SG2 and MK prepared upon hot-pressing at 1600°C.



**Fig. 4.**  $^{29}\text{Si}$  MAS NMR spectra SG1 (a) and MK (b) showing the presence of  $\text{SiC}_4$  and  $\text{SiO}_4$  signals. The  $^{29}\text{Si}$  MAS NMR spectrum of SG2 (not shown) exhibited the same features. No signals for  $\text{Si}_x\text{O}_{4-x}$  sites were observed in any of the samples, indicating that they are phase-separated.<sup>22</sup>

phase. Consequently, the molar fraction of the silica phase is  $\frac{z}{z+1/2}$ , that of  $\text{SiC}$  amounts  $\frac{x-y}{z+1/2}$  and the molar fraction of the segregated carbon is  $\frac{z-(x-y)}{z+1/2}$ . By taking the weight fractions of silica, silicon carbide, and excess carbon into account as well as their densities (i.e.,  $3.21 \text{ g/cm}^3$  for  $\text{SiC}$ ,  $2.2 \text{ g/cm}^3$  for vitreous silica, and  $1.45 \text{ g/cm}^3$  for carbon), the volume fractions of the individual phases were calculated (Table II).

The three SiOC samples strongly differ from each other with respect to their excess carbon content, which was determined to be  $\sim 0.4 \text{ vol}\%$  for SG1,  $5.9 \text{ vol}\%$  for SG2 and  $14.2 \text{ vol}\%$  for the MK sample. The sample with the highest amount of segregated carbon (i.e., MK) was found to exhibit a relatively low amount of carbidic carbon (i.e., carbon present within the glassy SiOC network or in form of  $\text{SiC}$  precipitates) with a Si:  $\text{C}_{\text{carbodic}}$  ratio of 5: 1; whereas SG1 and SG2 exhibited a higher carbidic carbon content (Si:  $\text{C}_{\text{carbodic}}$   $\sim 3$ : 1). As all samples are phase-separated, the carbidic carbon is considered to be present mainly as nano-sized  $\text{SiC}$  precipitates (see TEM micrographs in Fig. 5). The effect of the  $\text{SiC}$  phase on the HT creep behavior of the SiOC samples is of less significance,<sup>9</sup> due to the rather low volume content and the low aspect ratio of the  $\text{SiC}$  nanoparticles.<sup>8</sup> Therefore, we compared the creep behavior of SG1 and vitreous silica, to comment on the effect of the carbidic carbon; whereas the comparison between SG1 and SG2/MK focuses on the effect of the segregated carbon phase on their HT creep behavior.

The creep experiments were performed in compression at three different temperatures ( $1100^\circ\text{C}$ ,  $1200^\circ\text{C}$ , and  $1300^\circ\text{C}$ ) and applying three different stresses, that is, 10, 25, and 50 MPa. In Figs. 6(a)–(c) the creep curves for all three investigated samples at  $1300^\circ\text{C}$  are shown. The measured creep rates of the tested samples at all temperatures and stresses are summarized in Table III.

One should note that the used creep times are rather short (0.5 h) and thus the data (i.e., creep rates, activation energy) might not fully reflect the steady-state creep situation. To rationalize how strong the creep time affects the collected data, one long-term creep experiment with MK ( $1200^\circ\text{C}$ ) was performed. In Fig. 7, the strain rate is plotted as a function of the true strain. Obviously, the steady-state creep can be achieved, even if the value is normally reached at longer experimental time that used for the measurements in this study. However, one should note that there is only a secondary effect of the time on the creep rates (which differ from those determined upon using short creep time by only a factor of  $>2$ ; for example, at  $1200^\circ\text{C}$  and 25 MPa creep rates of

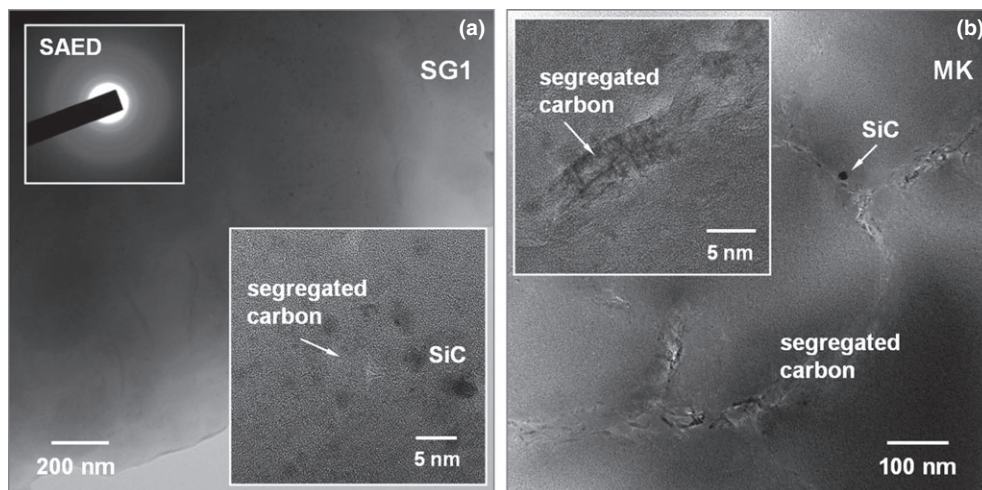


**Fig. 5.** TEM micrographs of a) SG1 and b) MK with low and high carbon content, respectively, upon creep at  $1300^\circ\text{C}$ . In SG1 a predominantly amorphous matrix is visible with only minor precipitation of  $\text{SiC}$  and a small fraction of segregated carbon. In contrast, the MK ceramic revealed a considerably higher content of segregated carbon (see Table II).

**Table II. Elemental Analysis Data and Chemical Compositions of the Prepared SiOC Samples**

	Element content (wt%)			Empirical formula	Volume fraction (vol%)		
	Si	O	C		SiO <sub>2</sub>	SiC	C <sub>xs</sub>
SG1	51.78	41.12	7.10	SiO <sub>1.39</sub> C <sub>0.32</sub> (SiO <sub>1.39</sub> C <sub>0.31</sub> + 0.01 C)	82.7	16.9	0.4
SG2	50.29	39.24	10.47	SiO <sub>1.37</sub> C <sub>0.49</sub> (SiO <sub>1.37</sub> C <sub>0.32</sub> + 0.17 C)	77.5	16.6	5.9
MK	45.11	41.9	12.99	SiO <sub>1.63</sub> C <sub>0.68</sub> (SiO <sub>1.63</sub> C <sub>0.19</sub> + 0.49 C)	77.5	8.3	14.2

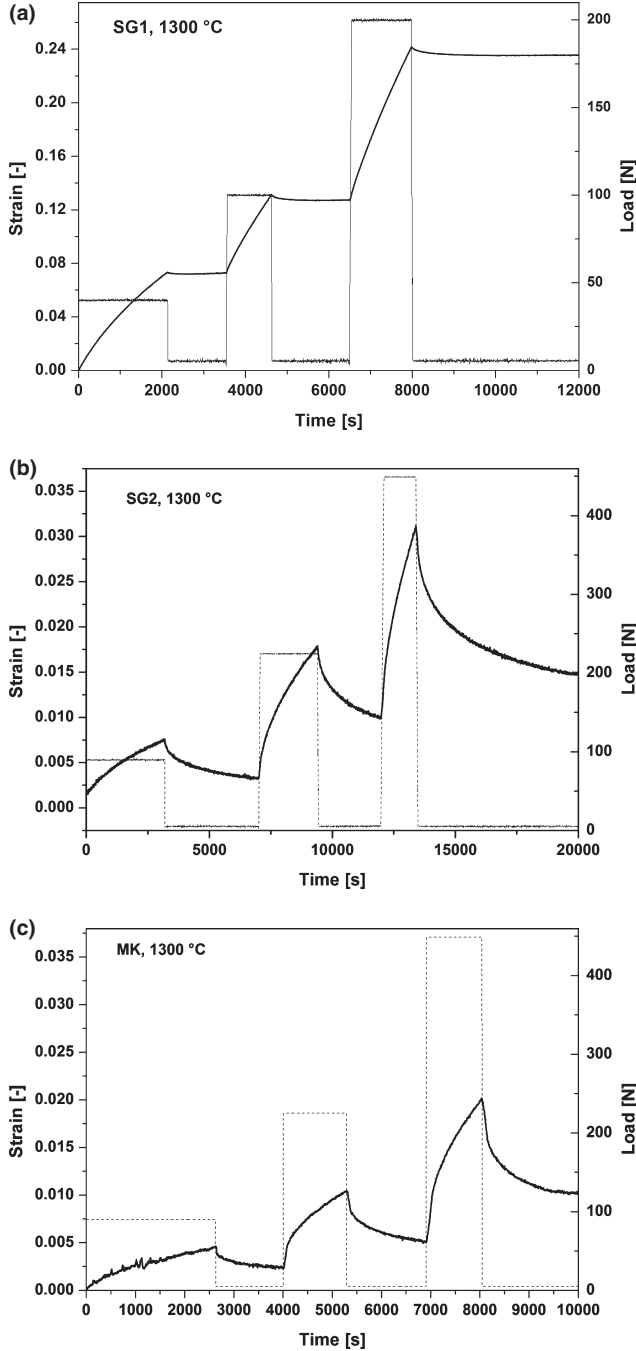


**Fig. 6.** Creep and recovery curves for samples SG1(a), SG2 (b) and MK(c) at 1300°C (as SG1 had different dimensions than those of SG2 and MK, different loads were applied to provide the same compression stress within all samples). Note the significant higher strains measured for SG1 as compared to SG2 and MK (scale of the left y-axis).

$6.17 \times 10^{-7}$  and  $3.67 \times 10^{-7} \text{ s}^{-1}$  were determined for creep times of 0.5 and 100 h, respectively). Thus, it can be considered that the creep curves from Fig. 6 disclose secondary

creep beyond the experimental time  $t_e^{(1)} \cong 1200 \text{ s}$  and, as consequence, the discussion of our data are meaningful despite the short creep times used within this study.

The analysis of the experimental data suggests that the 3-constant Jeffreys model [Eq. (1)], and the corresponding solution [Eq. (2)], are consistent with the recorded creep measurements. Despite the observed nonlinearities (in particular the existence of unrecoverable strain), the linear model [Eq. (1)] has the capability to catch the main rheological features of the samples; in particular, the evolution of the primary and secondary creep followed by a slow recovery.

The parameters of the model are obtained upon fitting the experimental data at the applied normal stress, that is, for  $\sigma_0 = 10 \text{ MPa}$ . As the creep behavior of SG2 and MK is similar, the calculations were only performed for samples SG1 and SG2. The results are shown in Table IV, where  $\eta_m = \eta_v = \eta_0$  was considered, and are represented in Fig. 8.

The values of the viscosity and elastic modulus corresponding to the model based on the Eq. (1) were computed with the formula:

$$\eta_0 = \frac{a \cdot \sigma_0}{2\dot{\epsilon}_{st}} \quad \text{and} \quad E = \frac{\eta_0}{2a} \quad (3)$$

The shear viscosities of the samples were calculated from the experimental strain rate versus stress data according to  $\eta = \frac{\sigma_0}{2\dot{\epsilon}(1+\nu)}$ ,<sup>7,23</sup> where  $\nu$  is the Poisson's ratio (0.11 for SiOC<sup>24</sup>).

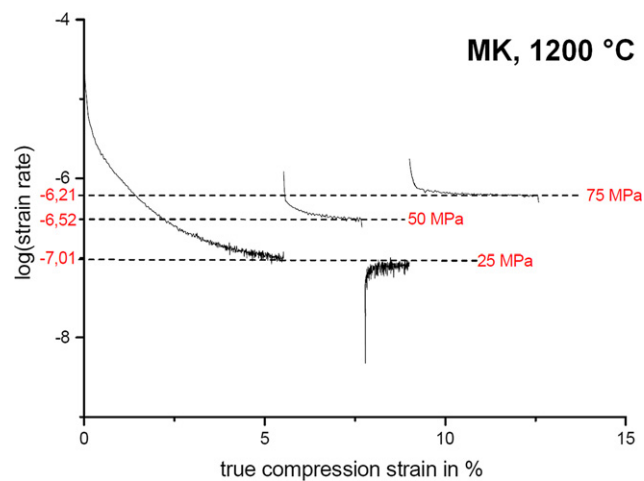
As expected, the results from Table IV underestimate the “static elasticity” of the samples, since the viscoelastic model (1) is designed for a fluid behavior. Thus, the calculated  $E$  moduli were up to three orders of magnitude lower than the experimental values measured under static conditions ( $10^{11}$  and  $1.1 \times 10^{11} \text{ Pa}$  for SG1 and SG2, respectively<sup>6,7</sup>). However, as the creep behavior of the SiOC sample was investigated at temperatures where the viscous flow is active, the  $E$  moduli (and the discrepancy between the modeled and the reported values thereof) are only of secondary importance for the discussion of the compression creep data.

It is important to remark that the recovery behavior is different for the sample SG1 as compared to SG2. As shown in Fig. 9, the recovery is almost absent for SG1, thus the fitting of the experimental data is only valid at times shorter than 120 s. Consequently, one can conclude that SG2 behaves more linear for the tested stress range and exhibits a higher elasticity as well as viscosity than the SG1 sample, which exhibits a more fluid-like behavior. These obvious differences in the rheology of the investigated samples give valuable insights into their nano/micro structure and are consistent with their phase compositions, as discussed below.

The reason for the pronounced difference between SG1 and SG2/MK is due to the significantly higher amount of segregated carbon present in SG2/MK. The volume fraction in SG1 (0.4 vol%) is remarkably lower than that in SG2 (5.9 vol%) and MK (14.2 vol%). This clearly affects the viscosity of the samples (i.e., the viscosity increases as the carbon content increases) as well as the activation energy, as also reported in our previous study<sup>9</sup>). Obviously, there might also be an effect of the silica content on the creep

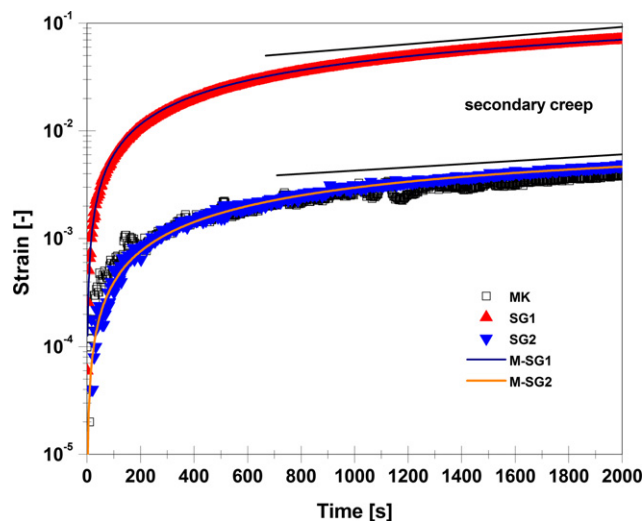
**Table III. Creep Rates of the Silicon Oxycarbide Samples at Different Temperatures and Stresses**

Sample	Temperature (°C)	Creep rate ( $10^{-8} \text{ s}^{-1}$ )		
		10 MPa	25 MPa	50 MPa
MK	1100	$4.38 \pm 0.56$	$4.90 \pm 0.75$	$5.29 \pm 0.29$
	1200	$10.3 \pm 0.12$	$36.7 \pm 0.43$	$74.2 \pm 0.34$
	1300	$113.0 \pm 1.2$	$337.0 \pm 2.1$	$751.0 \pm 2.2$
SG2	1100	$1.78 \pm 0.86$	$8.26 \pm 0.29$	$23.3 \pm 0.22$
	1200	$23.6 \pm 0.25$	$39.4 \pm 0.31$	$107.0 \pm 0.82$
	1300	$136.0 \pm 0.56$	$369.0 \pm 1.5$	$983.0 \pm 2.5$
SG1	1100	$19.2 \pm 0.15$	$21.5 \pm 0.15$	$36.4 \pm 0.31$
	1200	$279.0 \pm 0.75$	$385.0 \pm 1.8$	$622.0 \pm 1.9$
	1300	$2550 \pm 3.2$	$4780 \pm 5.6$	$6640.0 \pm 6.1$

**Fig. 7.** Logarithmic plot of the strain rate as a function of the true strain for MK at 1200°C and different pressures.

behavior of SiOC (which was shown to slightly decrease if comparing SG1 with SG2/MK); however, this effect should be considered as being marginal. Thus, as stated in Ref. [9], the effect of carbon is significantly stronger than that of the silica, due to the high aspect ratio of the former. Interestingly, we can observe two distinct effects of the carbon on the viscosity of SiOC (and its temperature evolution): By comparing in Figs. 10 and 11 the viscosity as well as the activation energy of vitreous silica and those of the single-phase SG1 sample (*non*phase-separated sample; data from literature<sup>7</sup>), one can conclude that the incorporation of carbon within the silica network (i.e., the presence of “carbide” carbon in SiOC) strongly increases its viscosity (and consequently the  $T_g$ , from 1170°C for vitreous silica to 1350°C–1400°C for single-phase SG1), while significantly reducing the activation energy from 712 kJ/mol for silica to 296 kJ/mol for single-phase SG1.

Furthermore, there is a large difference in the HT creep behavior between the SG1 prepared upon hot-pressing within this study (which is phase-separated) and the single-phase SG1 which was reported in the literature (having the same chemical composition, see<sup>7</sup>). The single-phase sample exhibits a significantly lower activation energy than the phase-sepa-

**Fig. 8.** Creep curves of samples SG1, SG2 and MK (1300°C, 10 MPa) as well as the fitted curves employing Eq. (2) and the material constants from Table IV.

rated sample (Figs. 10 and 11, Table V). Similarly, the  $T_g$  is strongly affected by the phase separation in SG1, since it decreases from 1350°C–1400°C in the single-phase sample<sup>7</sup> to 1250°C in the phase-separated material (Figs. 10 and 11). The reason why and in which manner the phase separation in SiOC glasses influences the activation energy and the viscosity is to date still unclear.

The samples having significant amount of segregated carbon (i.e., SG2, MK) exhibited  $T_g$  values and activation energies which were similar to those of single-phase SG1 (Table V, Fig. 11). One reasonable explanation is that the effect of the segregated carbon phase predominates in these samples. Since the behavior of the carbon can be considered as rather indifferent to the temperature under the studied conditions, the activation energy for creep of the SiOC/C composites might be “masked” by the carbon phase. Thus, the apparent values do not markedly differ from each other. Also the effect of the segregated carbon phase on the viscosity of the samples can be explained upon a “saturation” trend, as the viscosity of the SiOC/C composites cannot increase unlimited.

**Table IV. Material Constants Corresponding to the Rheological Model Based on the Eq. (1) for SG1 and SG2 Samples at 10 MPa and 1300°C (in the table are also inserted the steady values of the strain rate measured directly from the experiment)**

Sample	$\dot{\epsilon}_0$ (-)	$\dot{\epsilon}_{st}$ (-)	$a$ (s)	$\dot{\epsilon}$ (1/s)	$\dot{\epsilon}$ (1/s) - measured	$\eta_0$ (Pa s)	$E$ (Pa)
SG1	0.04	0.0145	630	$2.3 \times 10^{-5}$	$2.54 \times 10^{-5}$	$2.1 \times 10^{11}$	$1.6 \times 10^8$
SG2	0.0045	0.0009	900	$1.0 \times 10^{-6}$	$1.35 \times 10^{-6}$	$5.0 \times 10^{12}$	$2.7 \times 10^9$

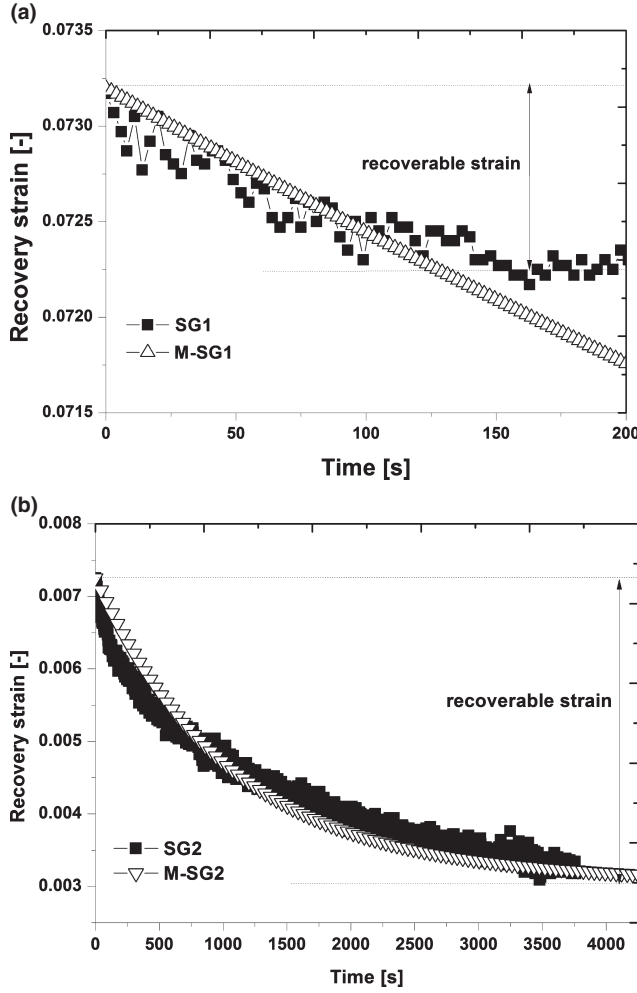


Fig. 9. Recovery strain from creep test, SG1 (a) and SG2 (b); the experimental data (full squares) are modeled by Eq. (2) and material parameters from Table IV (empty triangles).

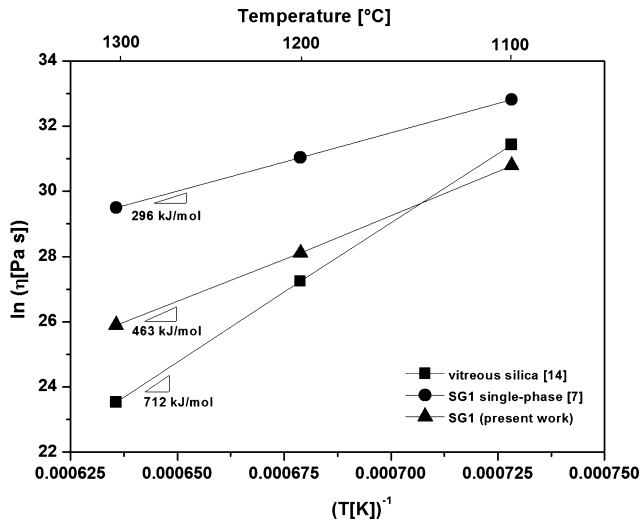


Fig. 10. Temperature evolution of the shear viscosity of vitreous silica, single-phase SG1 and phase-separated SG1 samples.

#### IV. Conclusions

The high-temperature creep behavior of SiOC glasses with three different contents of segregated carbon was investigated. The creep data were fitted using the Jeffreys viscoelastic model supporting the previously proposed microstructural model of SiOC glasses, which consist of a viscous silica and

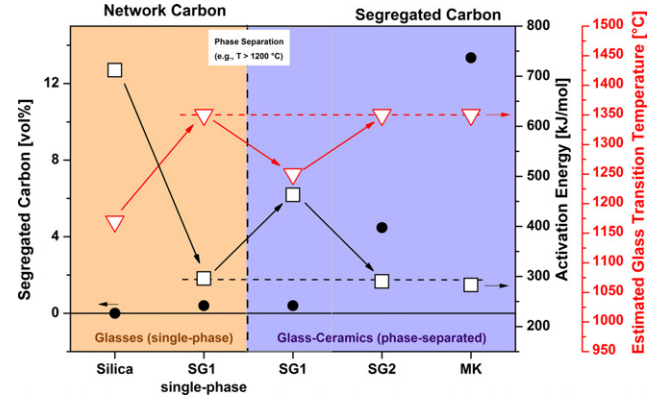


Fig. 11. Dependence of the activation energy (red triangles) and of the  $T_g$  values (black squares) on the volume fraction of segregated carbon (filled circles) in silicon oxycarbides (vitreous silica has been used besides SG1 as additional bench mark material for comparison, that is, 0 vol% segregated carbon<sup>14</sup>).

Table V. Activation Energies and  $T_g$  Values for Vitreous Silica and SiOC Samples

Sample	Activation energy for HT creep (kJ/mol)	Estimated $T_g$ (°C)
Vitreous silica	712 <sup>14</sup>	1170 <sup>14</sup>
SG1 (phase-separated)	463 (this work)	1250 (this work)
Single-phase SG1	296 <sup>7</sup>	1350–1400 <sup>7</sup>
(not phase-separated)		(extrapolated)
SG2 (phase-separated)	290 (this work)	1350 (this work)
MK phase-separated	283 <sup>9</sup>	1380–1400 <sup>9</sup>

an elastic carbon phase. Furthermore, a strong effect of the carbic carbon in SiOC glass (i.e., the carbon present within the glass network) on both the viscosity and the activation energy for creep was identified (as compared to vitreous silica). Also a significant influence of the network condition (i.e., single-phase versus phase-separated) on the creep behavior of SiOC was observed.

The results indicate that the creep behavior of SiOC glasses can be affected (and consequently improved) in two ways:

1. Single-phase SiOC glasses exhibit relatively large  $T_g$  values (1350°C–1400°C) and rather low activation energies for creep ( $\sim$ 280–300 kJ/mol) – they are materials of choice for near-zero-creep applications at HT.
2. Phase-separated SiOC glasses have significantly lower  $T_g$  values (i.e., 1250°C for phase-separated SG1) and larger activation energy for creep (463 kJ/mol) than those of their single-phase counterparts. Their creep behavior can be significantly improved by incorporation of segregated carbon. Interestingly, small contents of segregated carbon (e.g., 5.8 vol% as for SG2) are sufficient to lead to phase-separated SiOC samples with similar  $T_g$  and  $E_a$  values as compared to single-phase silicon oxycarbide. Thus, if high-temperature applications are anticipated (i.e., temperatures at which SiOC is prone to phase separation processes), SiOC compositions having excess carbon are mandatory to provide an improved creep resistance.

#### Appendix

##### Rationalization of the HT Creep Behavior of SiOC by the Jeffreys-1 Model for Viscoelastic Fluids

We have mentioned above that the Young's moduli of the SiOC samples modeled by the Jeffreys-1 model for viscoelas-

tic fluids were smaller than the experimental values by up to three orders of magnitude. Within this context, it is worth to remark that the measured elastic moduli of SiOC (values of  $\sim 10^{11}$  Pa<sup>6,7</sup>) characterize the behavior of the solid samples associated with their primary creep at zero strain rate. One possibility to explain the differences between modeled and experimental values of the elastic modulus is described in the following: During secondary creep, the internal microstructure is rearranged to a more solid-like configuration; as consequence, beyond a critical state (defined by the critical value of the strain at  $\sigma_0$ ) and for  $t > t_c^{(2)}$ , the sample exhibits again primary creep and the tendency to reach a constant value of the strain. In our interpretation, this means that in Fig. 1 the Saint Venant element connects an elastic element in parallel with the Jeffreys-1 model, therefore at  $t > t_c^{(2)}$  the material will answer similar to a Burgers 4-constants model. Hence, in steady state, that is, in the asymptotic limit of constant strain as  $t \rightarrow \infty$ , the measurable/experimental elastic modulus,  $E^*$ , is significantly larger than the modulus  $E$  obtained from the Jeffreys-1 model for viscoelastic fluids. The answers in creep at  $\sigma_0 = 10$  MPa of the Jeffreys-1 model for  $t < t_c^{(2)}$ , see M-SG1 curve in Fig. 8, and the answer of the Burgers model with  $E^* = 10^{11}$  Pa for  $t > t_c^{(2)}$ , are presented in Fig. A1 (for convenience, here  $t_c^{(2)} = 2000$  s, the value of experimental time corresponding to the critical value of deformation  $\epsilon_{cr}$ ).

The coupling of two rheological models is justified by the existence of a critical state of the deformation, which in our samples might be determined by the segregation of the two phases, that is, silica-rich and carbon phase.

We conclude that Jeffreys-1 model for viscoelastic fluids is appropriate to characterize the high-temperature creep behavior of the SiOC samples and gives the right values for the viscosity. As for infinite experimental creep time, the primary creep state might be reached again; in this case the use of the Burgers viscoelastic solid model seems to be more indicated.

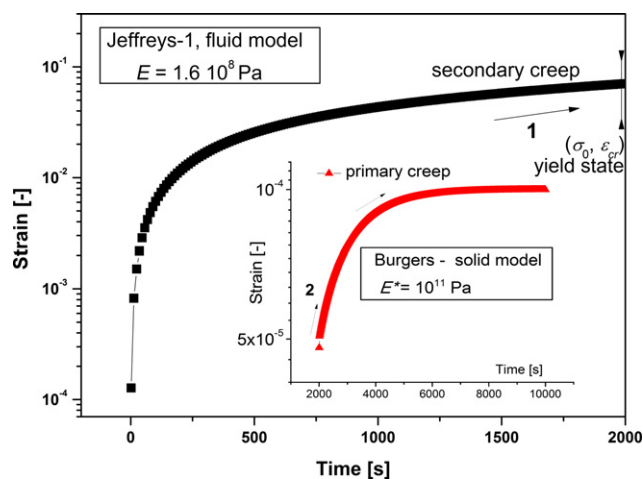


**Fig. A1.** Creep curves at  $\sigma_0 = 10$  MPa for the Jeffreys-1 model ( $0 \leq t \leq 2000$  s), and for the Burgers model ( $t > 2000$  s). At  $t = 2000$  s, the values of the strain and the strain rate are the same for both models (here the initial strain for the Burgers model has been considered zero).

### Acknowledgments

The authors thank Richard Günzler and Christoph Linck for the preparation of the samples as well as Dr. Hergen Breitzke for performing the <sup>29</sup>Si MAS

NMR measurements. Funding from DFG (IO 64/7-1, “High-Temperature Creep in SiOC-Based Glasses and Glass-Ceramics”) and from Ministry of Higher Education, Research and Arts in Hesse, Germany (Center of Excellence AdRIA) is gratefully acknowledged. CB acknowledges the financial support of TU Darmstadt and of the grant PN-II-ID-PCE-2012-4-0245 from UEFISCDI, Romania.

### References

- 1 R. Ellis, “Method of Making Electrically Conducting Glass and Articles Made Therefrom”; US Patent 2,556,616.
- 2 P. Colombo, G. Mera, R. Riedel, and G. D. Soraru, “Polymer-Derived Ceramics: 40 Years of Research and Innovation in Advanced Ceramics,” *J. Am. Ceram. Soc.*, **93**, 1805–37 (2010).
- 3 Y. D. Blum, D. B. MacQueen, and H. J. Kleebe, “Synthesis and Characterization of Carbon-Enriched Silicon Oxycarbides,” *J. Eur. Ceram. Soc.*, **25**, 143–9 (2005).
- 4 H. J. Kleebe and Y. D. Blum, “SiOC Ceramic with High Excess Free Carbon,” *J. Eur. Ceram. Soc.*, **28**, 1037–42 (2008).
- 5 A. Saha and R. Raj, “Crystallization Maps for SiCO Amorphous Ceramics,” *J. Am. Ceram. Soc.*, **90**, 578–83 (2007).
- 6 T. Rouxel, G. Massouras, and G. D. Soraru, “High Temperature Behavior of a Gel-Derived SiOC Glass: Elasticity and Viscosity,” *J. Sol-Gel. Sci. Technol.*, **14**, 87–94 (1999).
- 7 T. Rouxel, G. D. Soraru, and J. Vicens, “Creep Viscosity and Stress Relaxation of Gel-Derived Silicon Oxycarbide Glasses,” *J. Am. Ceram. Soc.*, **84**, 1052–8 (2001).
- 8 A. Scarmi, G. D. Soraru, and R. Raj, “The Role of Carbon in Unexpected Viscoelastic Behavior of Amorphous Silicon Oxycarbide Above 1273 K,” *J. Non-Cryst. Solids*, **351**, 2238–43 (2005).
- 9 B. Papendorf, E. Ionescu, H. J. Kleebe, C. Linck, O. Guillon, K. Nonnenmacher, and R. Riedel, “High-Temperature Creep Behavior of Dense SiOC-Based Ceramic Nanocomposites: Microstructural and Phase Composition Effects,” *J. Am. Ceram. Soc.*, **96**, 272–80 (2013).
- 10 E. Ionescu, H. J. Kleebe, and R. Riedel, “Silicon-Containing Polymer-Derived Ceramic Nanocomposites (pdc-ncs): Preparative Approaches and Properties,” *Chem. Soc. Rev.*, **41**, 5032–52 (2012).
- 11 S. Hampshire, R. A. L. Drew, and K. H. Jack, “Viscosities, Glass-Transition Temperatures, and Microhardness of Y-Si-Al-O-N Glasses,” *J. Am. Ceram. Soc.*, **67**, C46–7 (1984).
- 12 T. Rouxel, M. Huger, and J. L. Besson, “Rheological Properties of Y-Si-Al-O-N Glasses - Elastic-Moduli, Viscosity and Creep,” *J. Mater. Sci.*, **27**, 279–84 (1992).
- 13 R. K. Brow and C. G. Pantano, “Nitrogen Coordination in Oxynitride Glasses,” *J. Am. Ceram. Soc.*, **67**, C72–4 (1984).
- 14 R. H. Doremus, “Viscosity of Silica,” *J. Appl. Phys.*, **92**, 7619–29 (2002).
- 15 K. Ota and G. Pezzotti, “Internal Friction Analysis of Structural Relaxation in Si-C-O Glass,” *J. Non-Cryst. Solids*, **318**, 248–53 (2003).
- 16 A. Saha, R. Raj, and D. L. Williamson, “A Model for the Nanodomains in Polymer-Derived SiCO,” *J. Am. Ceram. Soc.*, **89**, 2188–95 (2006).
- 17 S. J. Widgeon, S. Sen, G. Mera, E. Ionescu, R. Riedel, and A. Navrotsky, “Si-29 and C-13 Solid-State nmr Spectroscopic Study of Nanometer-Scale Structure and Mass Fractal Characteristics of Amorphous Polymer Derived Silicon Oxycarbide Ceramics,” *Chem. Mater.*, **22**, 6221–8 (2010).
- 18 C. Linck, E. Ionescu, B. Papendorf, D. Galuskova, D. Galusek, P. Sajgalik, and R. Riedel, “Corrosion Behavior of Silicon Oxycarbide-Based Ceramic Nanocomposites Under Hydrothermal Conditions,” *Int. J. Mater. Res.*, **103**, 31–9 (2012).
- 19 E. Aulbach, R. Zuo, and J. Rodel, “Laser-Assisted High-Resolution Loading Dilatometer and Applications,” *Exp. Mech.*, **44**, 71–5 (2004).
- 20 C. Balan and C. Tsakmakis, “A Finite Deformation Formulation of the 3-Parameter Viscoelastic Fluid,” *J. Nonnewton. Fluid Mech.*, **103**, 45–64 (2002).
- 21 H. J. Kleebe, G. Gregori, F. Babonneau, Y. D. Blum, D. B. MacQueen, and S. Masse, “Evolution of C-Rich SiOC Ceramics - Part I. Characterization by Integral Spectroscopic Techniques: Solid-State NMR and Raman Spectroscopy,” *Int. J. Mater. Res.*, **97**, 699–709 (2006).
- 22 R. Kalfat, F. Babonneau, N. Gharbi, and H. Zarrouk, “Si-29 MAS NMR Investigation of the Pyrolysis Process of Cross-Linked Polysiloxanes Prepared from Polymethylhydrosiloxane,” *J. Mater. Chem.*, **6**, 1673–8 (1996).
- 23 L. A. An, R. Riedel, C. Konetschny, H. J. Kleebe, and R. Raj, “Newtonian Viscosity of Amorphous Silicon Carbonitride at High Temperature,” *J. Am. Ceram. Soc.*, **81**, 1349–52 (1998).
- 24 C. Moysan, R. Riedel, R. Harshe, T. Rouxel, and F. Augereau, “Mechanical Characterization of a Polysiloxane-Derived SiOC Glass,” *J. Eur. Ceram. Soc.*, **27**, 397–403 (2007). □